Electric-quadrupole interactions at ^{111}Cd in HfO_2 and ZrO_2: A perturbed angular correlation study

J. Luthin, K. P. Lieb, M. Neubauer, and M. Uhrmacher
II. Physikalisches Institut, Universität Göttingen, D-37073 Göttingen, Germany

B. Lindgren
Physics Department, University of Uppsala, Uppsala, Sweden

(Received 19 December 1997)

The electric hyperfine interactions of implanted ^{111}In/^{111}Cd probes in HfO_2 and ZrO_2 powder samples have been measured by means of perturbed angular correlation (PAC) spectroscopy, in the temperature range between 15 K and 1273 K and at various oxygen pressures. In both oxides, several electric-field gradients (EFG) have been established that show pronounced similarities among the two oxides. The EFG having the largest fraction at room temperature has been assigned to the substitutional, defect-free cation site. Its quadrupole frequency $\nu_Q = 112$ MHz and asymmetry parameter $\eta = 0.6$, at 300 K, are almost identical in both oxides. The scaling of this EFG relative to that found with ^{181}Hf/^{181}Ta probes in HfO_2 confirms the substitutional site. EFG calculations with the point charge and the cluster model for this site are compared with each other and with the data. The other EFG's observed have been attributed to different charge states of oxygen neighbor ions. Below 120 K, the spectra are strongly damped and indicate dynamic quadrupole interactions. [S0163-1829(98)00323-3]

I. INTRODUCTION

The present investigations of the hyperfine interactions of implanted ^{111}In ions in monoclinic HfO_2 and ZrO_2 powder samples evolved from our systematic studies on the electric-field gradients (EFG's) and magnetic hyperfine fields in binary and ternary oxides, carried out with perturbed angular correlation (PAC) spectroscopy. Among the questions recently addressed are the conditions under which the ^{111}Cd probe atoms, after implantation of the radioactive ^{111}In mother activity and annealings of the samples, reach substitutional, defect-free cation sites and in what way the electric-field gradients on these sites scale with the cation-oxygen bond lengths[1–4] as predicted by the point charge model (PCM) in ionic compounds. Other questions raised were the suitability of the PAC method to study structural or magnetic phase transitions in oxides,[5–7] the detection of implantation-induced or intrinsic defects,[8–10] the role of after-effects induced by the radioactive decay of ^{111}In,[11,12] and the possibility to study thermally activated charge-transfer reactions.[13,14] For many of these problems, PAC proved extremely useful to investigate the underlying structure or mechanism, and to interpret them on an atomic scale.

Very few PAC measurements have been carried out, however, in the monoclinic oxide structure typical for HfO_2 and ZrO_2 and only one with ^{111}In/^{111}Cd probes. In this lattice, there exists a single cation site, surrounded by seven oxygen ions at distances between 0.20 and 0.23 nm. A considerable number of measurements with the ^{181}Hf/^{181}Ta probe in HfO_2 (Refs. 15–22) has given a large fraction having an asymmetric EFG with the quadrupole frequency $\nu_Q = 707–807$ MHz. By virtue of introducing the radioactive probes via thermal neutron capture leaving little radiation damage, this fraction has been attributed to substitutional, defect-free cation sites. Furthermore, the PAC experiment on ^{181}Ta in monoclinic ZrO_2 (Ref. 23) has given evidence for a very similar EFG that, on the basis of the chemical and structural similarities between both compounds, was also attributed to the substitutional cation site. In three of the experiments, additional EFG's were observed.[21–23] The only PAC study on ^{111}Cd in ZrO_2 known to us is the one by Gardner *et al.*[24] who identified an asymmetric EFG with $\nu_Q = 83$ MHz at 1373 K, which is 70 K below the monoclinic-to-tetragonal phase-transition temperature.

The motivations of the present detailed study with ^{111}In/^{111}Cd probes in both oxides were first to identify the EFG at the substitutional site and to analyze its hyperfine parameters in relation to those found for ^{181}Ta probe nuclei and to theoretical estimates from the point charge and the cluster model. In addition we wanted to measure the EFG parameters over a large temperature range and to identify (and possibly interpret) other EFG's associated with defects.

II. EXPERIMENTAL PROCEDURE

The powder samples of HfO_2 had purities of either 99.57% (with contents of 0.1% ZrO_2 and 0.01% Al_2O_3, Fe_2O_3, and TiO_2) or 99.988% (with 0.01% ZrO_2), while the ZrO_2 powder samples had 99.975% purity. X-ray diffraction and energy dispersive x-ray analysis were used to check the monoclinic structure and stoichiometries of the samples. The powders were pressed into 0.5-mm-thick pellets of 4 mm diam at a pressure of some 10^7 Pa. The ^{111}In activity was implanted at 400 keV ion energy and at a total dose of about 10^{12} ions, by means of the Göttingen ion implanter IONAS.[25,26] The mass resolution of this implanter is good enough to select ions with mass number $A = 111$. As the implanting system has no Z resolution, ^{111}Cd produced in the β decay of ^{111}In before implantation also reached the

samples. The center of the tracer activity after implantation is at a depth of 70 nm, as estimated with the program TRIM95.[27] After doping, the samples were annealed at 1643 K for about 4 h making sure that radiation damage was removed, while less than 10% of the activity diffused out of the samples.

The PAC experiments were performed with several setups of four NaI(Tl) detectors in 90° geometry, connected to slow-fast circuits. The measurements below 315 K were carried out in a high vacuum chamber equipped with a closed-cycle helium cryostat (in the low-temperature range T_m=12–160 K) or a Peltier element (T_m=250–315 K). Measurements up to 773 K were carried out in air or at 5 $\times 10^{-3}$ Pa vacuum conditions. A special high-temperature PAC chamber, equipped with a heater made from pyrolytic boron nitride with a buried graphite layer, reached temperatures of up to T_m=1273 K.

Each PAC spectrum can be characterized by the perturbation function[28,29]

$$R(t)=2[N(180°,t)-N(90°,t)]/[N(180°,t)+2N(90°,t)] \quad (1)$$

and its Fourier transform A(ω). Here N(θ,t) denotes the coincidence rate of two detectors positioned at Θ=90° or 180° relative to each other and t denotes the time interval elapsed between detecting the 171-keV start γ ray and the 245-keV stop γ ray. These two radiations mark the times of population and decay of the 245-keV isomeric state in ^{111}Cd, which has a mean lifetime of t=123 ns. Most spectra have been fitted, by assuming *static* EFG's and using the expression

$$R(t)=A_2^{eff}\Sigma f_i G_{22}^{(i)}(t). \quad (2)$$

Up to four fractions f_i (i=1–4) were necessary to achieve good fits to the data, each fraction being characterized by its perturbation factor,

$$G_{22}^{(i)}(t)=\sum_{n=0}^{3} S_{2n}(\eta_i)\cos(g_n(\eta_i)\nu_{Qi}t) \times \exp[-(g_n(\eta_i)\delta_i t)^2/2]d(g_n(\eta_i)\nu_{Qi}t,\tau_R). \quad (3)$$

The ith traceless EFG tensor is characterized by the quadrupole frequency $\nu_{Qi}=eQV_{zz}^{(i)}/h$ and the asymmetry parameter $\eta_i=(V_{xx}^{(i)}-V_{yy}^{(i)})/V_{zz}^{(i)}$. The exponential damping factor $\exp[-(g_n(\eta_i)\delta_i t)^2/2]$ accounts for a Gaussian distribution of quadrupole frequencies around ν_{Qi} having a width δ_i. The function $d(g_n(\eta_i)\nu_{Qi}t,\tau_R)$ accounts for the damping of $G_{22}^{(i)}(t)$ due to the final time resolution τ_R of the apparatus. For further details and the coefficients S_{2n} and g_n, see Refs. 28 and 29. Some of the strongly damped perturbation functions were fitted with exponential functions $R(t)=A_2^{eff}\exp(-\lambda t)$, where the damping constant λ is a measure for the reciprocal fluctuation time of the relevant EFG.[29]

III. RESULTS IN HFO_2

Table I summarizes the PAC measurement conditions in HfO_2, including the range of measuring temperatures T_m and pressure of each run. In order to check the results obtained in the various temperature ranges and in order to study the possible influence of the oxygen activity, several overlapping runs have been carried out, both under identical measuring conditions and for different oxygen activities or temperature cycles. Figures 1 and 2 exhibit typical experimental and fitted $R(t)$ functions and their Fourier transforms, which illustrate the evolution of the hyperfine interactions in this compound. The parameters are listed in Table II. Up to about 100 K, very weak oscillations in the $R(t)$ functions are seen giving rise to a broadly distributed frequency spectrum. At 125 K, a quadrupole frequency triplet EFG_1 emerges that

TABLE I. Summary of experimental conditions during the PAC measurements in HfO_2.

Sample	Measuring temperature T_m (K)	Atmosphere
1	15–325	10^{-3} Pa
2	25–400	10^{-3} Pa
3	33–293	10^{-3} Pa
4	293–643	10^{-3} Pa
5	293–724	10^{-3} Pa
6	293–970	10^{-3} Pa
7	254–313	air
8	293 and 1274	air and CO/CO_2 mixture
9	673–873	air
10	673–1173	air
11	873–1074	air

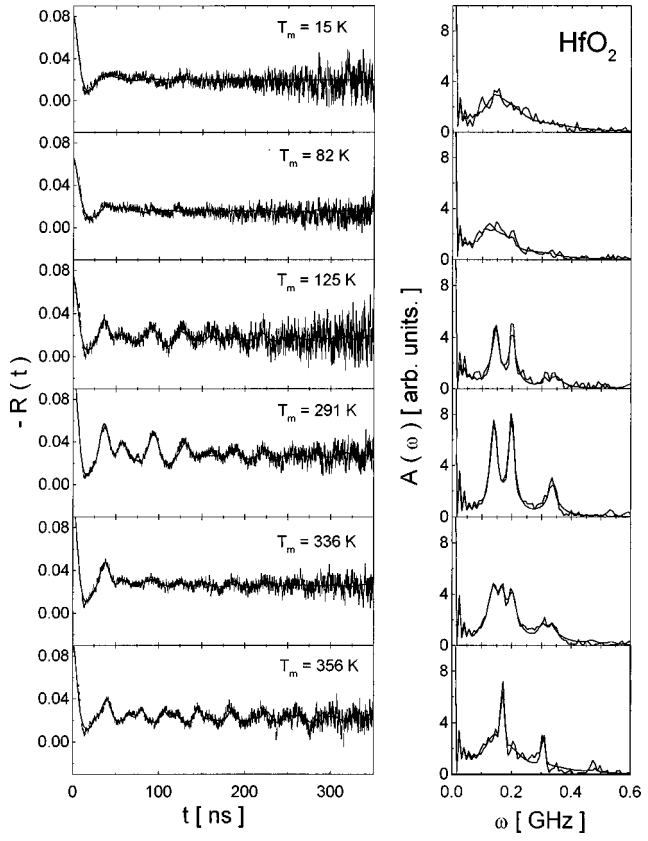

FIG. 1. PAC spectra and their Fourier transforms for ^{111}Cd in HfO_2 measured at 15–356 K in vacuum.

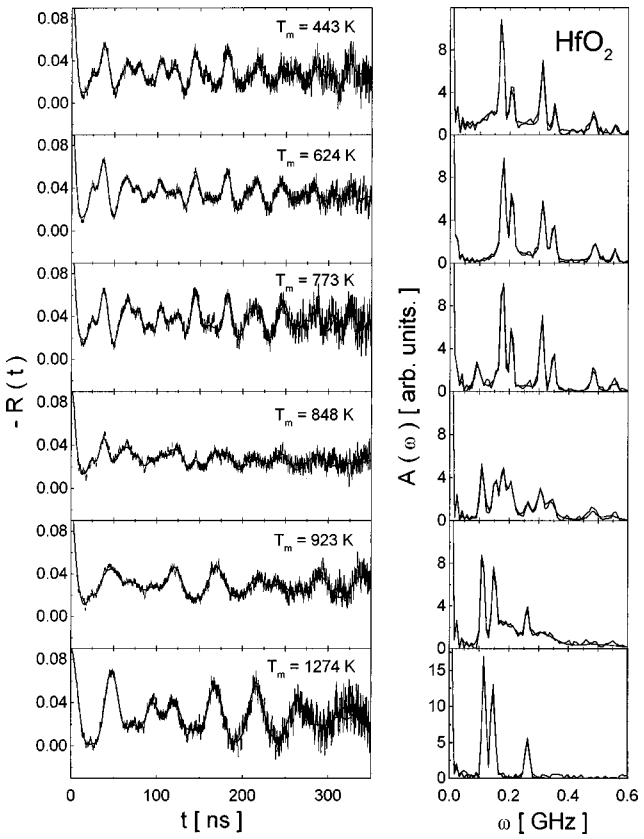

FIG. 2. PAC spectra and their Fourier transforms for ^{111}Cd in HfO_2 measured at 443–1274 K in air.

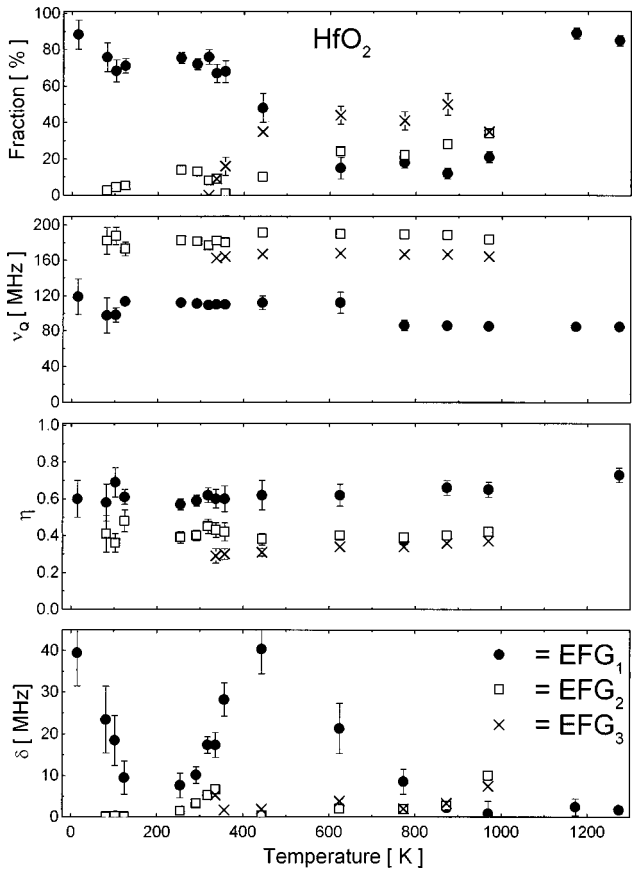

FIG. 3. Temperature dependence of all fitted PAC parameters for ^{111}Cd in HfO_2.

increases in sharpness and intensity up to about room temperature. The frequency spectrum then becomes broader again and, at 356 K, a new frequency triplet EFG_2 arises that, above 443 K up to 773 K, is accompanied by the well-defined EFG_3. At the very highest temperatures T_m=923–1274 K, another well-defined EFG_4 (small δ_4) evolves, having similar hyperfine parameters as EFG_1 and reaching a very large fraction of f_4=90%.

TABLE II. Measured electric-field gradients for ^{111}Cd in HfO_2 and ZrO_2.

Site i	T_m (K)	ν_{Qi} (MHz)	η_i	δ_i (MHz)	f_i (%)
		HfO_2			
1	254	112(2)	0.57(3)	8(3)	75(3)
2	254	181(2)	0.39(3)	14(3)	
	970	184(5)	0.42(4)	35(5)	
3	313	168(3)	0.30(3)	6(3)	
	970	165(5)	0.42(4)	35(5)	
4	970	85(3)	0.65(4)	21(3)	
	1173	84(3)	0.71(4)	≈3	89(3)
		ZrO_2			
1	250	112(2)	0.64(4)	9(4)	75(5)
2	250	190(3)	0.33(4)	≈2	8(4)
	673	180(3)	0.35(4)	5	30(5)
3	373	160(3)	0.28(4)	2	45(5)
	673	168(3)	0.40(4)	5	32(5)
4	1173	82(3)	0.66(4)	≈3	100

The temperature dependence of the relevant parameters is summarized in Fig. 3. We note moderate changes of the parameters ν_{Qi} and η_i, but strong variations of the fractions f_i and distribution widths δ_i. For that reason, we have given, in Table II, the EFG parameters at those measuring temperatures T_m, where the corresponding fractions f_i are relatively large and the distribution widths δ_i small.

In the temperature range T_m=600–1000 K, we noted appreciable differences of some EFG parameters measured in vacuum (at 5×10^{-3} Pa) and in air. We therefore decided to take few further runs in which the oxygen activity $a(O_2)=p(O_2)/[p(O_2)_{air}]$ was adjusted by means of a CO/CO_2 mixture. According to the Boudouard equilibrium, the oxygen activity follows the relationship

$$\log_{10}a(O_2)=2\log_{10}[p(CO_2)/p(CO)]-29532\ \mathrm{K}/T+9.188. \quad (4)$$

In the measuring cycle illustrated in Fig. 4, we took first PAC spectra at T_m=1274 K, $a(O_2)$=1 and $a(O_2)=3.9\times10^{-12}$, then turned to room temperature, returned to T_m=1274 K, $a(O_2)=6\times10^{-16}$ and again to room temperature. Figure 4 clearly shows that all spectra at 1274 K show well-defined EFG's that are almost identical among themselves, but markedly differ from those taken at room temperature. The two quadrupole interactions EFG_1 and EFG_4

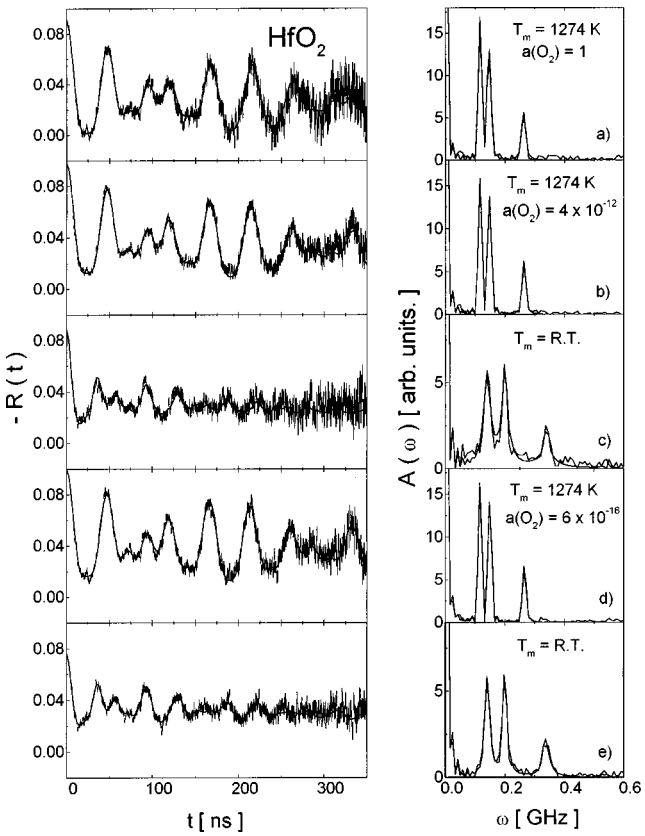

FIG. 4. Dependence of the PAC spectra on the oxygen activity and temperature. The spectra were taken in consecutive order.

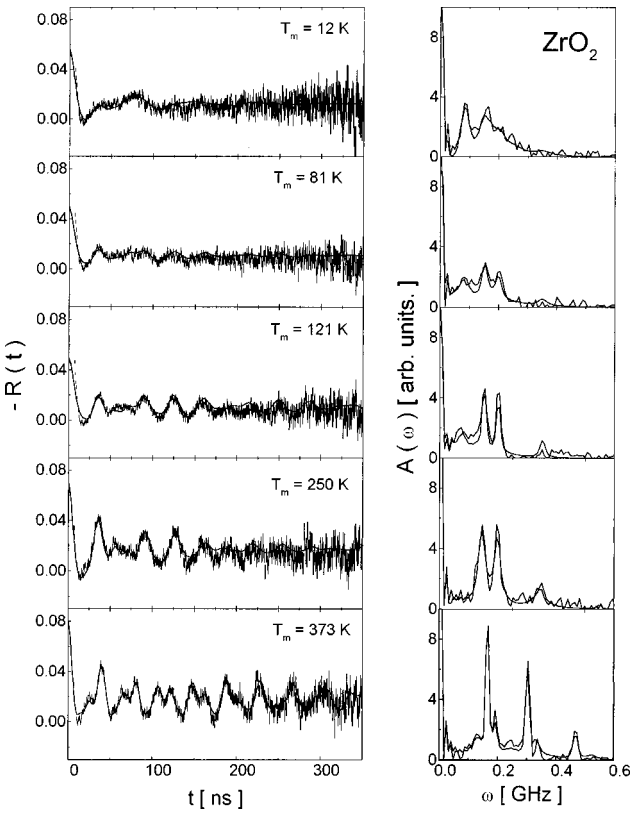

FIG. 5. PAC spectra and their Fourier transforms for ^{111}Cd in ZrO_2 measured at 12–373 K in vacuum.

are thus well distinguishable and *independent* of the oxygen activity; the transformation between them being reversible.

IV. RESULTS IN ZrO_2

PAC measurements in ZrO_2 were carried out at temperatures T_m in the range from 12 K to 1173 K. The samples of the runs up to 573 K were kept in vacuum and those above in a nitrogen atmosphere. The evolution of the perturbation functions $R(t)$ and Fourier transforms $A(\omega)$ is very similar to the case of HfO_2, as illustrated in Figs. 5 and 6. In ZrO_2, four EFG's with nonvanishing quadrupole frequencies were identified, in addition to a small fraction with $\nu_Q = 0$. The EFG parameters are summarized in Table II, and their evolution with the temperature T_m is shown in Fig. 7.

The broadly distributed frequencies below 100 K are followed by a well-defined EFG_1 at 120–300 K (see Fig. 5) with the fraction f_1 reaching almost 80% at 250 K. As in the case of HfO_2, the interactions EFG_2 and EFG_3 appear in the range $T_m = 370$–900 K and have small δ values. Above 600 K, they decrease in intensity and give rise to EFG_4 having hyperfine parameters very similar to those of EFG_1. Although the asymmetry parameter of this latter fraction equals η_1, its lower frequency $\nu_{Q4} = 80$ MHz markedly differs from the value $\nu_{Q1} = 112$ MHz, typical in the low-temperature regime. The quadrupole parameters of EFG_4 agree with those reported in Ref. 22 which were taken at 1373 K. The two frequencies ν_{Q1} and ν_{Q4} are essentially constant in the temperature ranges where they are well defined, nevertheless a linear decrease with the temperature dependence can be fit-

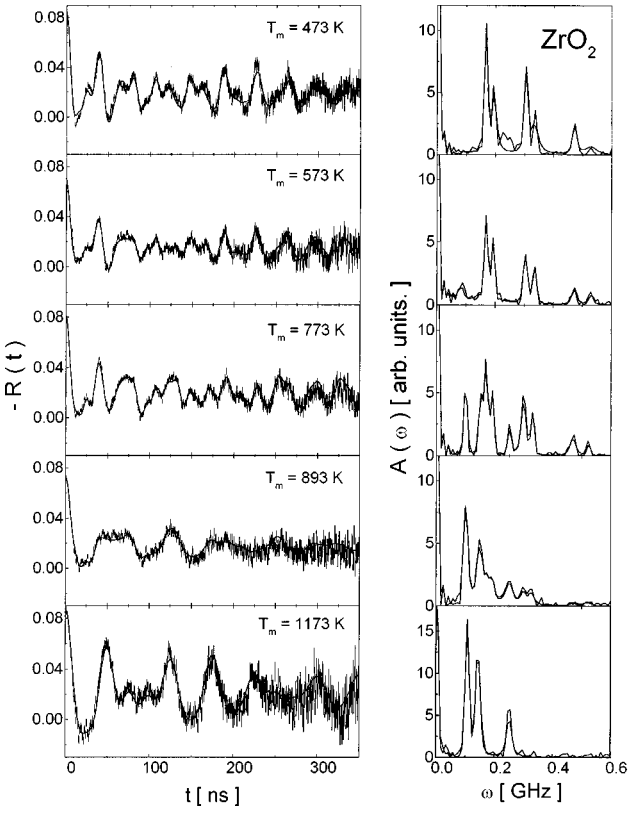

FIG. 6. PAC spectra and their Fourier transforms for ^{111}Cd in ZrO_2 measured at 473–1173 K in air.

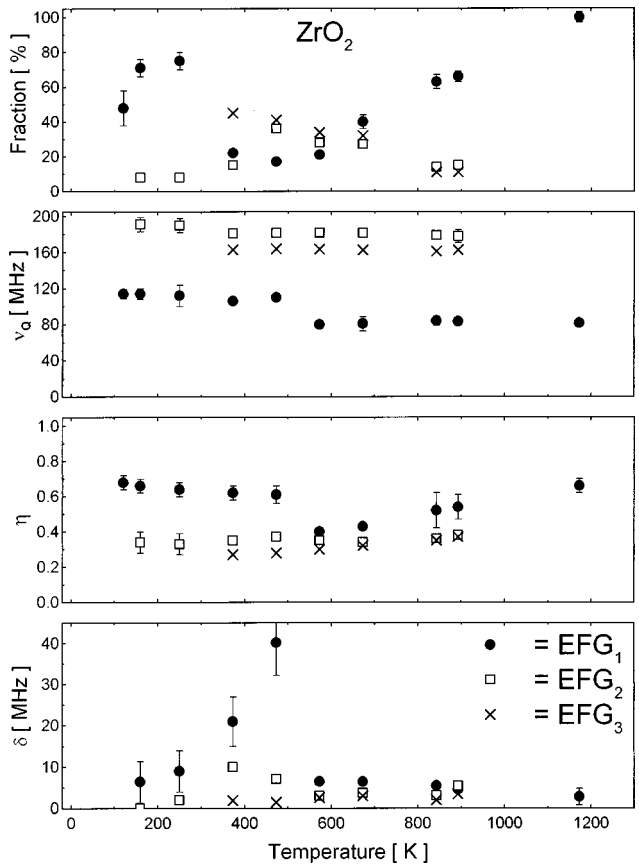

FIG. 7. Temperature dependence of all fitted PAC parameters for ^{111}Cd in ZrO_2.

ted, as in the case of HfO_2 for both PAC probes, keeping in mind the large δ_1 values in the transitional region.

V. DISCUSSION

In spite of their high spatial resolution concerning the immediate neighborhood of the probe atoms and their power to clearly distinguish between various defect configurations, PAC measurements lack an intrinsic calibration of the hyperfine fields, whenever the probe atom is an impurity, as it is in the present study. Arguments of ion valences, preferred oxygen coordinations, and cation-oxygen bond lengths and the like are used to assign the site of the probe atoms. In favorable cases, comparisons with intrinsic probe atoms, the results of other hyperfine techniques or model calculations may help to solve this problem.

A. Substitutional cation site in the monoclinic lattice

We will first argue that both EFG_1 and EFG_4 refer to the same microsurrounding that we attribute to the substitutional, defect-free cation site of the monoclinic lattice of HfO_2 and ZrO_2. In a first step we inspect the PAC results obtained in previous measurements with ^{181}Hf/^{181}Ta probes: in HfO_2, the radioactive mother isotope ^{181}Hf surely is at the cation site. In the spirit of the point charge model (PCM) the EFG's obtained with different PAC probes should scale, according to their quadrupole moments Q and Sternheimer factors γ_∞, via the relationship

TABLE III. Comparison of measured EFG's for ^{181}Ta and ^{111}Cd in HfO_2 and ZrO_2.

T_m (K)	ν_{Q1} (MHz)	η_i	$\nu_Q(^{181}\text{Ta})/\nu_Q(^{111}\text{Cd})$	Ref.
		^{181}Ta in HfO_2		
77	807(8)	0.35(3)	7.3(2)	15
300	801	0.28(27)	7.2	16
300	784	0.35(16)	7.1	17
300	762(11)	0.37	6.9(2)	18
300	627	0.36	5.6	19
300	707(1)	0.36(11)	6.4(1)	20
300	789(6)	0.35(1)	7.1(1)	21
300	707(6)	0.34(3)	6.4(2)	22
1173	720	0.49	8.6(1)	22
		^{111}Cd in HfO_2		
254	112(2)	0.58(2)		present work
313	111(2)	0.60(3)		,,
1173	84(3)	0.71(4)		,,
		^{181}Ta in ZrO_2		
293	722(6)	0.33	6.5(1)	21
1323	650	0.43		23
		^{111}Cd in ZrO_2		
250	112(2)	0.64(4)		present work
1373	83	0.69		24

$$\nu_Q = eQV_{zz}/h. \tag{5}$$

Assuming that the largest EFG component V_{zz} is proportional to the lattice contribution $V_{zz}^{latt}(1-\gamma_\infty)$, we expect the ratio of quadrupole frequencies of $\nu_Q(^{181}\text{Ta})/\nu_Q(^{111}\text{Cd})=6.5(10)$, using the known quadrupole moments Q (^{181}Ta)=2.36(5) (b) and Q (^{111}Cd)=0.83(13) (b),[28] as well as the Sternheimer factors $\gamma_\infty(^{181}\text{Ta})=-68.12$ and γ_∞ (^{111}Cd)=−29.27.[30]

We first compare the measured EFG_1 for ^{111}Cd in both oxides with that for ^{181}Ta. Table III summarizes these frequency ratios $\nu_{Q1}(^{181}\text{Ta})/\nu_{Q1}(^{111}\text{Cd})$. The fact that all frequency ratios are in good agreement with the predicted value of 6.5(10) and that the quadrupole frequencies for both probes agree with each other in both matrices, strongly supports our conjecture that EFG_1, indeed, is related to probes at undisturbed cation sites.

The main argument for identifying EFG_4 with EFG_1 is the behavior of the fractions during reversible changes of the measuring temperature T_m, which is illustrated in Fig. 8. In the temperature range 300–800 K up to 30% of the substitutional ^{181}Hf/^{181}Ta probes observe a change of their microsurrounding [Fig. 8(a)],[22] giving rise to EFG_3. The PAC parameters of fraction f_3 give a frequency factor of 6.1(5) (see Table III). The decrease of the substitutional fraction f_1 is much more dramatic for ^{111}In/^{111}Cd probes [Figs. 8(b) and 8(c)]: f_1 nearly completely disappears in favor of fraction f_3, which is observed with ^{181}Hf/^{181}Ta probes, too, and of fraction f_2, seen only with ^{111}In probes. In all three cases the decrease of f_1 starts around 300 K. An interpretation of the fractions f_2 and f_3 as being due to trapped defects will be further discussed in Sec. V C.

At this point we note that, for ^{181}Hf/^{181}Ta in HfO_2, the substitutional fraction f_1 recovers around 700 K and in-

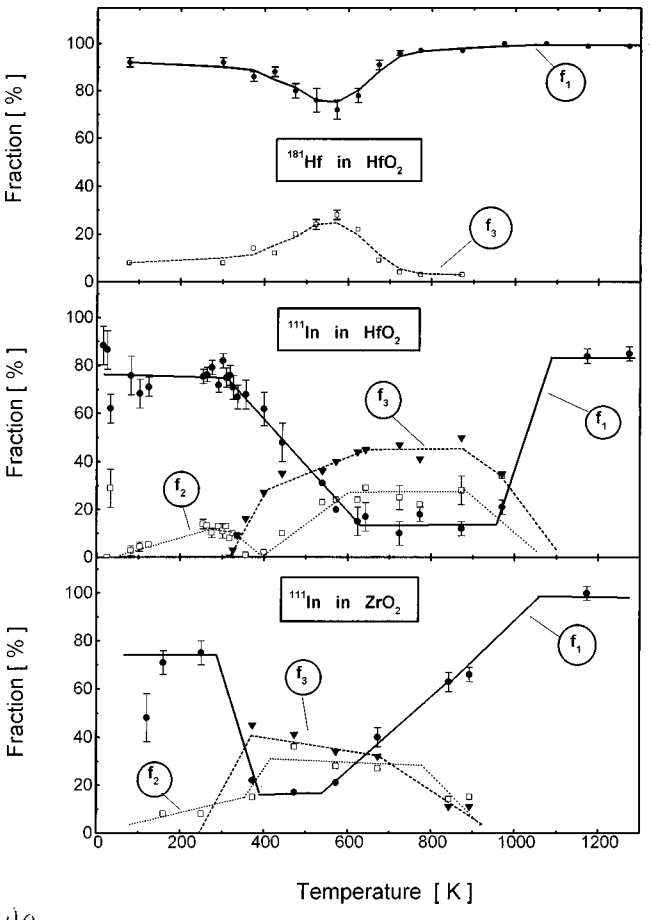

FIG. 8. Comparison of the temperature dependence of the substitutional fraction f_1/f_4 and the defect fractions f_3 and f_2 for ^{111}In probes in HfO_2 and ZrO_2 with ^{181}Hf probes in HfO_2. All lines are given only to guide the eye.

creases to 100%. In spite of the scatter of the hyperfine parameters at room temperature (see Table II), we emphasize the slight decrease of ν_{Q1} and the increase of η_1 at 1173 K, relative to their values at 300 K for both oxides. Guided by these observations, we suggest that the fractions f_4 for ^{111}In/^{111}Cd in both HfO_2 and ZrO_2 also denote the substitutional site. Nevertheless, it has to be remarked that at high temperatures (1173 K) the frequency factor is found to be 8.6(1) (see Table III).

Additional support for our assumption that EFG_1 and EFG_4 originate from the same site comes from PAC studies in CoO (Ref. 9) and NiO (Ref. 8) by Wenzel and co-workers. At high temperatures, a large number of intrinsic point defects has to be expected. However, these defects are not trapped for sufficiently long times at the probes to generate static EFG's. Consequently, the fast EFG fluctuations cancel and the EFG of the unperturbed lattice remains. The EFG at the highest temperatures should therefore be identified with the unperturbed lattice.

B. Calculations of the lattice EFG in HfO_2 and ZrO_2

1. Point charge model

A systematic comparison of measured electric-field gradients of ^{111}Cd probes in ionic binary metal oxides with the

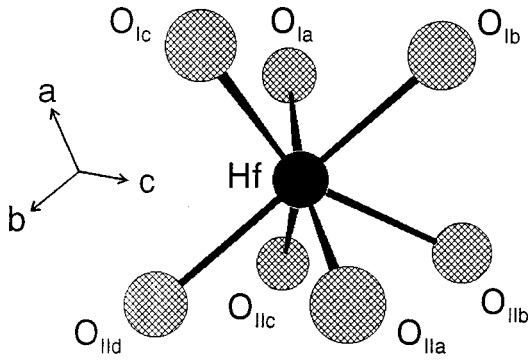

FIG. 9. Positions and nomenclature of the seven oxygen atoms that are the next neighbors to the cation Hf or Zr. The direction of the axes of the unit cell are also given.

predictions of the PCM performed by Bartos and co-workers[1,2] and by Wiarda *et al.*[4] has shown that the PCM reproduces the asymmetry parameter on substitutional sites whenever the cation-oxygen bond length exceeds $d_{M\text{-}O}\approx 0.2$ nm. The PCM calculations also reproduce the quadrupole frequencies ν_Q in the bixbyite In_2O_3 (where the ^{111}In probe atoms are on lattice sites, of course), but disagrees as to the extent to which the bond length $d_{M\text{-}O}$ deviates from the In-O bond length. On the basis of the PCM, Bartos and co-workers[1,2] and Lupascu *et al.*[3] have been able to refine the coordinates in bixbyite oxides to a precision of the order of 10 pm. Below $d_{M\text{-}O}\approx 0.2$ nm, the PCM was found to fail,[4,31] probably due to local deformations induced by the oversized ^{111}Cd ion. A recent extensive PAC investigation by Attili *et al.*[32] for ^{111}Cd in ternary oxides of the delafossite structure ($A^{1+}B^{3+}O_2$) has given further evidence for these findings.

Figure 9 illustrates the oxygen coordinations of Hf (and Zr) in monoclinic HfO_2 (and ZrO_2).[33,34] There are two groups of oxygen ions that have small differences in their $d_{M\text{-}O}$ values: group *Ia*, *Ib*, *Ic* has $d_{M\text{-}O}=0.203$–0.217 nm, while group *IIa*–*IId* has $d_{M\text{-}O}=0.215$–0.228 nm at room temperature. All bond lengths thus exceed the critical value $d_{M\text{-}O}=0.2$ nm above which the PCM should work in ionic oxides. Table IV lists the measured and calculated EFG parameters ν_Q and η for both probes in both compounds, assuming the Sternheimer factors and quadrupole moments quoted above and extending the lattice sums over all ions within 5 nm. The PCM underestimates the quadrupole frequencies ν_{Q1} (^{181}Ta) and ν_{Q1} (^{111}Cd) by a factor of 1.26–1.85 in both oxides. As often in PCM calculations the asymmetry parameter η_1 for ^{111}Cd in HfO_2 is perfectly predicted. But while the measured asymmetry parameter in ZrO_2 is in perfect agreement with that in HfO_2, the PCM predicts a much smaller value for ZrO_2. Such a discrepancy is quite unusual and we tried to find out which coordinates in the lattice are responsible for it. It turned out that the coordinate responsible for the position of the three oxygen ions *Ia*–*Ic* shifts η between 0.2 and 0.8 if the value is exchanged between HfO_2 and ZrO_2. The coordinates used for calculating the lattice sum have been determined using x-ray diffraction.[33,34] As the atomic numbers of Zr and O differ strongly, the reflexes of O are hard to identify among the Zr reflexes. We suggest that the O (*I*) coordinate in the data set of ZrO_2 (Refs. 33 and 34) is not correct. The smaller difference between the calculated and measured asymmetry pa-

TABLE IV. Comparison of measured EFG's for ^{181}Ta and ^{111}Cd in HfO_2 and ZrO_2 with predictions of cluster calculations and the point charge model (PCM).

	Cluster Calculation			PCM		Experiment	
System	V_{zz} 10^{17} C cm^{-2}	ν_Q (MHz)	η	ν_Q MHz	η	ν_Q^{exp} MHz	η^{exp}
^{181}Ta in HfO_2	12.6(1.0)	721(60)	0.9(1)	420	0.62	789(6)	0.35(1)
^{111}Cd in HfO_2	−3.1(1.0)	62(20)	0.8(2)	65	0.62	111(2)	0.60(3)
^{181}Ta in ZrO_2	−12.9(2.1)	736(120)	0.6(3)	564	0.19	722(6)	0.33
^{111}Cd in ZrO_2				89	0.19	112(2)	0.64(4)

rameter η_1 in the case of ^{181}Ta in both oxides is not explained.

2. Cluster calculations

The theoretical basis for the electronic-structure calculations is the self-consistent one-electron local-density formalism in the Hartree-Fock-Slater model. This is solved with the discrete variational method (DVM).[35] Details of the method have been previously published[36] and only a short review of the numerical procedure is given here. A double variational basis was composed of numerically calculated neutral and ionized atoms. Core orbitals were frozen, i.e., the cores were only present in the overlap matrix but not in the Hamiltonian matrix. No muffin tin or other spherical shape restrictions of the potential was enforced and the Hedin-Lundqvist exchange correlation potential[37] was adopted. From the obtained wave functions the self-consistent charge density $\rho(\vec{r})$ was calculated and all the nine components of the EFG tensor (in atomic units):

$$V_{ij} = -\int \rho(\vec{r}) \frac{3r_i r_j - \delta_{ij} r^2}{r^5} d\vec{r} + V_{ij} \text{ (nuclear)} \qquad (6)$$

where the second term is a summation over the nuclear or ionic pointlike charges with the same geometric weight factor as in the first term. Here V_{ij} refers to the cluster coordinate system. After diagonalization the dominant EFG component V_{zz} and the asymmetry parameter η are obtained (Table IV).

The smallest possible clusters were used, TaO_7 and CdO_7 (see Fig. 9) with interatomic distances appropriate for HfO_2 and ZrO_2, respectively. Point charge lattice summations show that more than 80% of the EFG originate from these seven nearest oxygen ions. The ionized clusters were embedded in a charged, spherical shell to ensure a charge neutral system. A more accurate treatment would have been to embed the cluster in a pseudopotential appropriate for the ionic crystal. Instead calculations were performed for different cluster charges. The EFG's listed in Table IV are the average values using $(TaO_7)^{7-}$, $(TaO_7)^{9-}$, $(TaO_7)^{11-}$ and $(CdO_7)^{8-}$, $(CdO_7)^{10-}$, $(CdO_7)^{12-}$, respectively. The uncertainties, within parenthesis, represent half the maximum deviation. The formal chemical valence of Ta^{5+} and O^{2-} correspond to $(TaO_7)^{9-}$. However, a Mulliken[38] population analysis of the self-consistent wave functions gives $O^{1.5-}$ increasing to $O^{1.8-}$ for $(TaO_7)^{11-}$. Similarly, the O ionicity of $(CdO_7)^{12-}$ is only −1.6. Consequently, any *a priori* assumption of the cluster charges is not possible.

The large value of the asymmetry parameter η implies that there are two components of the EFG, almost equal in amplitude but with different sign. Since V_{zz} by definition is the largest component, a small change in lattice coordinates may flip the sign as for Ta in HfO_2 and ZrO_2 in Table IV. However, this change of sign is more likely due to the given uncertainty of the calculations. The PAC experiments cannot determine the sign of the EFG.

3. Comparison

The calculated main component of the Ta EFG's agrees quite well with the experimental values regarding that these calculations do not depend on any Sternheimer factor γ_∞. The PCM assumes a fully ionized Ta probe ion while the cluster calculations show a considerable EFG contribution from the valence electrons. However, this valence contribution is often proportional to the lattice-ion EFG in the PCM making ratios such as the asymmetry parameter η more reliable in the PCM. The cluster calculations here show too large η values.

The calculated Cd EFG is by almost a factor of 2 smaller than the experimental value. A relaxation of the O sites around the Cd impurity probe ion may be expected and may also be the reason for the discrepancy in the EFG. Different relaxed positions of the O ions were tested and changed the EFG considerably. The values given in Table IV correspond to unrelaxed O sites appropriate for the unperturbed host. Nevertheless, the result support the site identification of the main fraction of the PAC signal as being a substitutional site without O vacancies.

C. Defect EFG's in HfO_2 and ZrO_2

As already mentioned in the previous section we attribute the fractions f_2 and f_3 to the trapping of defects close to the probe on the cation site. The reasoning is based on the observation that 80–100% of the impurity probe ^{111}In/^{111}Cd trap such defects (f_3 and f_2), whereas only 20% of the self-atom ^{181}Hf/^{181}Ta do so (f_3). Nevertheless, one has to realize that all samples had been well annealed at very high temperatures (T_a=1673 K): the defects are therefore likely to be intrinsic ones. In the following we will use the notation of Krüger/Vink.[39] X_Z^Y denotes an ion X or a vacancy ($X=V$) on the lattice site of the ion Z in a perfect lattice. Y gives the effective charge, compared to the nominal charge on that

TABLE V. PCM calculations of different effective charges on the oxygen next neighbors (all interaction frequencies are given in MHz).

	Eff. charge: +1			Eff. charge: +2		
Position	ν_Q (PCM)	η (PCM)	$1.7*\nu_Q$	ν_Q (PCM)	η (PCM)	$1.7*\nu_Q$
O_{IId}	219	0.28	372	391	0.16	665
O_{Ic}	203	0.23	345	383	0.13	651
O_{IIc}	164	0.28	279	318	0.16	541
O_{IIa}	154	0.71	262	308	0.36	524
O_{Ib}	193	0.28	328	401	0.15	682
O_{Ia}	202	0.52	343	403	0.26	685
O_{IIb}	83	0.45	141	103	0.33	175
		f_3			f_2	
Experiment:		0.32	168(3)		0.40	190(3)

lattice site. Positive effective charges are marked with points (•), negative charges with ($'$); $Y=x$ corresponds to a charge difference of zero. An electron hole is symbolized by $h^{\bullet}$.

The most probable equilibrium defects in HfO_2 and ZrO_2 are either doubly charged oxygen vacancies $(V_O)^{\bullet\bullet}$ and mobile electrons e', according to the reaction

$$(O_O^{2-})^x \Leftrightarrow (V_O)^{\bullet\bullet} + 2e' + 1/2O_2, \tag{7}$$

or fully ionized cation vacancies $(V_M)'''' $ (M=Hf or Zr) and mobile electron holes $h^{\bullet}$, according to the reaction

$$(M_M^{4+})^x + 1/2O_2 \Leftrightarrow (V_M)'''' + 4h^{\bullet} + MO_2. \tag{8}$$

The mobile charge carriers are needed for charge compensation as both oxides only slightly deviate from stoichiometry.[40] In general, the concentration of both types of equilibrium defects decreases at lower temperatures, but this effect is faster for the oxygen vacancies.[41–44] Furthermore, the formation enthalpy for cation vacancies is only 0.11(1) eV as compared to 1.67(18) eV for oxygen vacancies.[40] Therefore, the presence of cation vacancies seems to be most probable in the measured temperature range 300–800 K. In reaction (8) the electron holes are much more mobile compared to ionic vacancies, and we expect mainly electron holes to be trapped close to the probes.

We have tried to model the observed defect EFG's using the PCM. Since the EFG is only sensitive to the charge attached to a certain lattice site, one cannot distinguish between a charged oxygen vacancy or a differently charged oxygen ion. Using the above-mentioned arguments we calculated the defect EFG's by localizing one or two electron holes at one of the next-neighbor oxygen ions. The calculated values ν_Q (PCM) and η (PCM) are given in Table V. In its third column ν_Q (PCM) is multiplied by the factor 1.7 found in the calculation of the substitutional site. Although there is only one substitutional cation site in the monoclinic lattice, the low lattice symmetry causes different EFG's for charged defects on each different oxygen ion. Most calculated values are by far too large as compared to the experimental values of ν_{Q3} and ν_{Q2}. Only for the atom O_{IIb} do the calculated values of ν_Q (PCM) and η (PCM) match the data for the two assumed charge states. It is surprising that just one site should be favored, but it is this oxygen site that disturbs the octahedral coordination of oxygen ions around the ^{111}In probe. Similar calculations have been made for both charge states of all 10 possible single cation vacancies close to the probe. Only 3 out of 20 cases agree with one of the experimental frequencies ν_{Q3} or ν_{Q2}, but fail completely in the prediction of the experimental asymmetry parameter. We conclude that ν_{Q3} and ν_{Q2} are probably caused by one and two electron holes trapped at the oxygen ion O_{IIb} next to a probe atom.

Finally, we discuss the reversible temperature behavior of the two defect EFG's. At high temperatures, the holes are not trapped during the PAC observation time of 400 ns, but are trapped and released at a very high rate. A similar situation has been described in detail by Wenzel, Uhrmacher, and Lieb for ^{111}In/^{111}Cd in CoO.[8] In such a situation of a high fluctuation rate, the lattice EFG emerges and individual defects are not observable any more. The behavior at temperatures below 300 K is less easily explained. One may assume that at these temperatures other traps are more attractive for electron holes than the oxygen atom O_{IIb} next to the probe.

D. Low-temperature behavior of the PAC spectra

The low-temperature behavior of the observed PAC spectra in HfO_2 and ZrO_2 as shown in Figs. 1 and 5 was not investigated in great detail. The spectra up to 120 K are strongly damped and have been fitted assuming a broad frequency distribution around ν_{Q1}. In HfO_2 the width δ_1 increases up to 40 MHz at the lowest temperature T_m=15 K. On the other hand, at this temperature one might identify in the Fourier spectra a new frequency triple (see Fig. 1), indicating another EFG. Strong damping at low temperatures and the reappearance of defined frequencies at low temperatures remind us of results in La_2O_3 (Ref. 11) and In_2O_3 (Ref. 12). Both effects have been explained in these cases by assuming dynamical hyperfine interactions related to the electron capture decay of ^{111}In and to a low availability of electrons to quickly restore the stable ^{111}Cd electron shell. We propose the existence of similar phenomena in HfO_2 and probably in ZrO_2, too, but the present data are not sufficient for further analysis.

VI. CONCLUSIONS

The most prominent result of the present PAC study with ^{111}In/^{111}Cd probes implanted into monoclinic, polycrystal-

line HfO_2 and ZrO_2 is that, after the high-temperature annealings, all ^{111}In atoms appear to reside on substitutional cation sites. The EFG parameters measured at room temperature for this site, $\nu_{Q1}=112(2)$ MHz, $\eta_1=0.62(3)$, are in perfect agreement in both compounds and highlight the identical crystallographic structure. Measurements performed in the intermediate temperature range from 300 to 900 K evidenced two further EFG's that we attribute to defective environments. We have presented some arguments that they may be connected with the trapping and detrapping of one or two electron holes at the site of that oxygen neighbor (O_{IIb}) that most disturbs the octahedral symmetry around the ^{111}In probe. One similar fraction was previously found in ^{181}Hf-PAC experiments in HfO_2, with only up to 30% in intensity, besides the substitutional defect-free site. There are indications of dynamic hyperfine interactions below 120 K.

The measured EFG parameters for substitutional ^{111}Cd have been compared with that found for ^{181}Ta/^{181}Hf probes in both oxides and with predictions of the PCM and the cluster model. With regard to the ^{181}Ta probes, the PCM reproduces well the measured frequency ratio of 7.1(1) in HfO_2 and 6.5(1) in ZrO_2, respectively, as well as the asymmetry parameter $\eta_1=0.62$ for ^{111}Cd in HfO_2. The 20–40% deviations of the predicted quadrupole frequencies for both probe nuclei in both compounds must also be regarded as a fair success of the PCM. There are, on the other hand, a number of rather severe discrepancies, in particular, the strong deviations of the predicted η values for ^{111}Cd in ZrO_2 and for ^{181}Ta in both compounds, as well as the obvious decrease of the quadrupole frequencies by 25%, which occurs in both ^{111}In-doped oxides around 600 K. As the PCM often has been found to reproduce the asymmetry of the EFG in ionic oxides, we argue that the different PCM predictions of this quantity in the two oxides may either be due to errors in the determination of the position of the oxygen ions (via x-ray diffraction analysis), or to slight distortions of the oxygen coordination by the impurities. Refined x-ray or neutron diffraction measurements would be useful to clarify this point. In addition, the cluster calculations indicate that both oxides show a fair amount of covalent bonding (up to 20%), which sheds some doubt on the validity of the PCM calculations.

ACKNOWLEDGMENTS

The authors are indebted to Dr. L. Ziegeler and D. Purschke for their help in preparing the samples and implanting the ^{111}In activity. J.L. thanks the Physics Department of the University of Uppsala for the hospitality extended to him during his visit. This work has been supported by Deutsche Forschungsgemeinschaft (Li325/2).

[1] A. Bartos, D. Wiarda, M. Uhrmacher, and K. P. Lieb, Phys. Lett. A **157**, 513 (1991); Hyperfine Interact **80**, 953 (1993).
[2] A. Bartos, K. P. Lieb, M. Uhrmacher, and D. Wiarda, Acta Crystallogr., Sect. B: Struct. Sci. **49**, 165 (1993).
[3] D. Lupascu, A. Bartos, K. P. Lieb, and M. Uhrmacher, Z. Phys. B **93**, 441 (1994).
[4] D. Wiarda, M. Uhrmacher, A. Bartos, and K. P. Lieb, J. Phys.: Condens. Matter **5**, 4111 (1993).
[5] Z. Inglot, K. P. Lieb, M. Uhrmacher, T. Wenzel, and D. Wiarda, Z. Phys. B **87**, 323 (1992).
[6] D. Wiarda, T. Wenzel, M. Uhrmacher, and K. P. Lieb, J. Phys. Chem. Solids **53**, 1199 (1992).
[7] M. Uhrmacher, R. N. Attili, K. P. Lieb, K. Winzer, and M. Mekata, Phys. Rev. Lett. **76**, 4829 (1996).
[8] T. Wenzel, M. Uhrmacher, and K. P. Lieb, Philos. Mag. A **72**, 1099 (1995).
[9] T. Wenzel, K. P. Lieb, and M. Uhrmacher, J. Phys. Chem. Solids **55**, 683 (1994).
[10] Th. Wichert, Hyperfine Interact. **15/16**, 355 (1983).
[11] D. Lupascu, S. Habenicht, K. P. Lieb, M. Neubauer, M. Uhrmacher, and T. Wenzel, Phys. Rev. B **54**, 871 (1996).
[12] S. Habenicht, D. Lupascu, M. Uhrmacher, L. Ziegeler, and K. P. Lieb, Z. Phys. B **101**, 187 (1996).
[13] A. F. Pasquevich, M. Uhrmacher, L. Ziegeler, and K. P. Lieb, Phys. Rev. B **48**, 10 052 (1993).
[14] M. Neubauer, A. Bartos, K. P. Lieb, D. Lupascu, M. Uhrmacher, and T. Wenzel, Europhys. Lett. **29**, 175 (1995).
[15] E. Gerdau, J. Wolf, H. Winkler, and J. Braunsfurth, Proc. R. Soc. London, Ser. A **311**, 197 (1969).
[16] P. R. Gardner and W. V. Prestwich, Can. J. Phys. **48**, 1430 (1970).
[17] Y. Yeshurun and B. Arad, J. Phys. (France) **7**, 430 (1974).
[18] H. Barfuss, G. Böhnlein, H. Hohenstein, W. Kreische, H. Niedrig, H. Appel, R. Heidinger, J. Raudies, G. Then, and W.-G. Thies, Z. Phys. B **47**, 99 (1982).
[19] A. Baudry, P. Boyer, and P. Vulliet, Hyperfine Interact. **13**, 263 (1983).
[20] S. Koicki, M. Manasijevic, and B. Cekic, Hyperfine Interact. **14**, 105 (1983).
[21] M. C. Caracoche, J. A. Martinez, P. C. Rivas, and A. Lopez-Garcia, Hyperfine Interact. **39**, 117 (1988).
[22] A. Ayala, R. Alonso, and A. Lopez-Garcia, Phys. Rev. B **50**, 3547 (1994).
[23] M. C. Caracoche, M. T. Dova, A. R. Lopez-Garcia, J. A. Martinez, and P. C. Rivas, Hyperfine Interact. **39**, 117 (1988).
[24] J. A. Gardner, H. Jaeger, H. T. Su, W. H. Warnes, and J. C. Haygarth, Physica B **150**, 223 (1988).
[25] M. Uhrmacher, K. Pampus, F. J. Bergmeister, D. Purschke, and K. P. Lieb, Nucl. Instrum. Methods Phys. Res. B **9**, 234 (1985).
[26] M. Uhrmacher, M. Neubauer, W. Bolse, L. Ziegeler, and K. P. Lieb, Nucl. Instrum. Methods Phys. Res. B (to be published).
[27] J. P. Biersack (private communication).
[28] G. Schatz and A. Weidinger, *Nuclear Solid State Physics* (Wiley, New York, 1996).
[29] H. Frauenfelder and R. M. Steffen, in *Alpha, Beta and Gamma-Ray Spectroscopy* (North-Holland, Amsterdam, 1965).
[30] R. M. Sternheimer, Phys. Rev. A **6**, 1702 (1972).
[31] T. Wenzel, A. Bartos, K. P. Lieb, M. Uhrmacher, and D. Wiarda, Ann. Phys. (Leipzig) **1**, 155 (1994).
[32] N. Attili, M. Uhrmacher, K. P. Lieb, L. Ziegeler, M. Mekata, and E. Schwarzmann, Phys. Rev. B **53**, 600 (1996).

[33] R. Ruh and P. W. R. Corfield, J. Am. Ceram. Soc. **53**, 126 (1970).
[34] R. E. Hann, P. R. Suitch, and J. L. Pentecost, J. Am. Ceram. Soc. **68**, C-285 (1985).
[35] D. E. Ellis and G. S. Painter, Phys. Rev. B **2**, 2887 (1970).
[36] B. Lindgren, Phys. Rev. B **34**, 648 (1986).
[37] L. Hedin and B. I. Lundqvist, J. Phys. C **4**, 2064 (1971).
[38] R. S. Mulliken, J. Chem. Phys. **23**, 1833 (1955).
[39] F. A. Kröger and H. J. Vink, Solid State Phys. **3**, 307 (1956).
[40] P. Kofstad, in *High Temperature Corrosion* (Elsevier Applied Science, New York, 1988).
[41] P. Kofstad and D. J. Ruzicka, J. Electrochem. Soc. **110**, 181 (1963).
[42] J. Xue and R. Dieckmann, Adv. Ceram. Mater. **24**, 106 (1993).
[43] H. Solmon, J. Chaumont, C. Dolin, and C. Monty, Adv. Ceram. Mater. **24**, 12 (1993).
[44] J. Xue, J. Electrochem. Soc. **138**, 36C (1991).